geosciences

MDPI

Article

New Occurrence of Pyroxenites in the Veria-Naousa Ophiolite (North Greece): Implications on Their Origin and Petrogenetic Evolution

Aikaterini Rogkala [1,*], Petros Petrounias [1], Basilios Tsikouras [2] and Konstantin Hatzipanagiotou [1]

[1] Section of Earth Materials, Department of Geology, University of Patras, 265 00 Patras, Greece; galaxy_hotel_kefalonia@hotmail.gr (P.P.); k.hatzipanagiotou@upatras.gr (K.H.)
[2] Faculty of Science, Physical and Geological Sciences, Universiti Brunei Darussalam, Jalan Tungku Link, Bandar Seri Begawan, Gadong BE1410, Brunei Darussalam; basilios.tsikouras@ubd.edu.bn
* Correspondence: krogkala@upatras.gr; Tel.: +30-2610-99-6288

Received: 6 June 2017; Accepted: 13 September 2017; Published: 21 September 2017

Abstract: The Veria-Naousa ophiolite represents a dismembered unit in north Greece, which includes variably serpentinised lherzolite and harzburgite, locally intruded by a sparse network of dykes or thin layers of websterite and olivine-orthopyroxenite composition. The websterite and the olivine-orthopyroxenite show abundant petrographic and geochemical evidence (relic olivines with mantle affinities, Cr-rich spinels, low Al_2O_3, depletions in incompatible elements, and concave upwards rare earth element patterns) that they comprise replacive bodies from refractory subarc mantle precursors. The occurrence of these pyroxenites in dykes implies that channelled percolation of melts account for their replacive character. High CaO/Al_2O_3, low Zr and crystallisation of diopside suggest that a melt of ankaramitic/carbonatitic composition percolated in lherzolite replacing porphyroclastic olivine and forming the pyroxenes in the websterite. At a shallower level, harburgites were impregnated by boninitic melts (inferred by U-shape rare earth element patterns and very rich in Cr spinels) triggering the replacement of porphyroclastic olivine by orthopyroxene for the formation of olivine-orthopyroxenite. These peritectic replacements of olivine commonly occur in a mantle wedge regime. The peculiar characteristics of the Veria-Naousa pyroxenites with LREE and compatible elements enrichments resemble the subarc pyroxenites of Cabo Ortegal implying a similar environment of formation. Whole-rock and mineralogical (spinel and clinopyroxene) compositions are also in favour of a backarc to arc environment. It is recommended that the evolution of the Veria-Naousa pyroxenites record the evolution of the subarc region and the opening of a backarc basin in a broad SSZ setting in the Axios Zone of eastern Greece.

Keywords: pyroxenite; marginal basin; melt-rock reaction; Veria-Naousa ophiolite

1. Introduction

Subduction-related and subduction-unrelated ophiolites [1] form in a variety of tectonic settings including oceanic spreading centres, backarc and forearc basins, arcs and other extensional magmatic settings including those in association with plumes [2–6]. The chemical composition of ophiolitic rocks is commonly used for recognising a variety of different tectonic settings, as well as the nature of mantle sources. The ophiolites that form as a result of subduction initiation processes host of a sequence of igneous rocks formed by a magma source that changed progressively in composition by the combined effects of melt depletion and subduction-related metasomatism [7,8].

Pyroxenites with variable modal contents of olivine, garnet and spinel, ranging in composition from orthopyroxenite through websterite to clinopyroxenite are important constituents of the upper mantle, usually forming veins, layers, or dykes in peridotites [9–12]. Mantle-derived

pyroxenites also occur as xenoliths in alkali basaltic or kimberlitic lavas, commonly associated with peridotites [13,14]. They are genetically diverse and may have formed initially in the mantle, the oceanic or even in the continental crust. Usually, mantle pyroxenites are interpreted as precipitates from asthenosphere-derived melts that passed through the lithospheric mantle [15]. A small number of these formed as high-pressure, pyroxenitic cumulates [10,15]. This rock type is of great importance for the genesis of mid-ocean ridge basalt [16], ocean-island basalt [17–19], and arc magmas [20]. Moreover, pyroxenite may be the missing link to explain the imbalance between the compositions of continental crust and primary arc magmas [21,22], therefore it may play a key role in global dynamic processes.

Numerous studies are associated with diverse pyroxenites, which are commonly distributed in the upper mantle. These rocks do not only influence mantle heterogeneity but also act as inferred source materials of ocean island arc and mid-ocean ridge basalts [23–26]. Pyroxenites are considered to be a significant component in the Earth's mantle, yet their genesis remains controversial [27,28]. They can be "secondary" products of reaction between mantle peridotite and infiltrating melts, which may be derived from recycled crustal components or from the melting of ambient peridotite [18,29,30]. The genesis of mantle pyroxenites is divided into three categories: high pressure cumulates from basaltic magmas passing through the mantle, solid-state remnants of subducted oceanic crust and metasomatic products resulting from the interaction of pervasive melts with mantle peridotites [18,21,31]. Modal mineralogy and primary mineral compositions of the upper mantle pyroxenites are considered as a key to constrain the extent of partial melting, fluid phase enrichment and mantle-melt interaction processes subsequent to melt extraction [32].

In this study, we present for the first time textural, petrographic, mineralogical and geochemical features of mantle pyroxenites from the Veria-Naousa ophiolite aiming at constraining their genesis and the geodynamic processes during their formation.

2. Geological Setting

Extensive fieldwork in the Veria-Naousa ophiolitic complex focused mainly on the distribution and mode of development of the ophiolitic rocks, as well as their relation to the adjacent formations. These rocks extend throughout the area between Veria and Naousa towns and belong to the Almopias subzone of the Axios geotectonic zone, in northern Greece (Figure 1). They represent remnants of oceanic lithosphere which were thrust from one or more ocean basins and have been obducted onto Late Triassic-Jurassic platform carbonates of the Pelagonian Zone during Upper Jurassic to Lower Cretaceous [33–37]. The ophiolite is a dismembered suite and includes, from base to top, serpentinised lherzolite and harzburgite, intruded by a sparse network of pyroxenitic dykes, as well as gabbro, diabase and pillow basalt. The serpentinised peridotites are intensely tectonised, showing a dense network of joints. Rare rodingite dykes occur in the serpentinised ultramafic rocks. Neogene to Quaternary sedimentary formations (conglomeratic limestone, breccia limestone, flysch) lie uncomfortably on the ophiolite. A granite to granodiorite body, of unknown age, penetrates serpentinised peridotites near the village of Trilofos (Figure 1). A cataclastic zone of diabasic fragments and albitite veins is observed along the eastern contact of the ophiolite with the Pelagonian carbonate rocks (Figure 1).

Pyroxenites are the least abundant rock units among the Veria-Naousa ultramafic section. Websterite and Olivine-orthopyroxenite (Ol-orthopyroxenite) form tectonically disrupted dykes or thin layers up to 1 m thick and a few tens of meters long, within serpentinised harzburgite. The small sizes of the pyroxenite outcrops render their mapping difficult; hence, their occurrences are indicated on the geological map with stars (Figure 1).

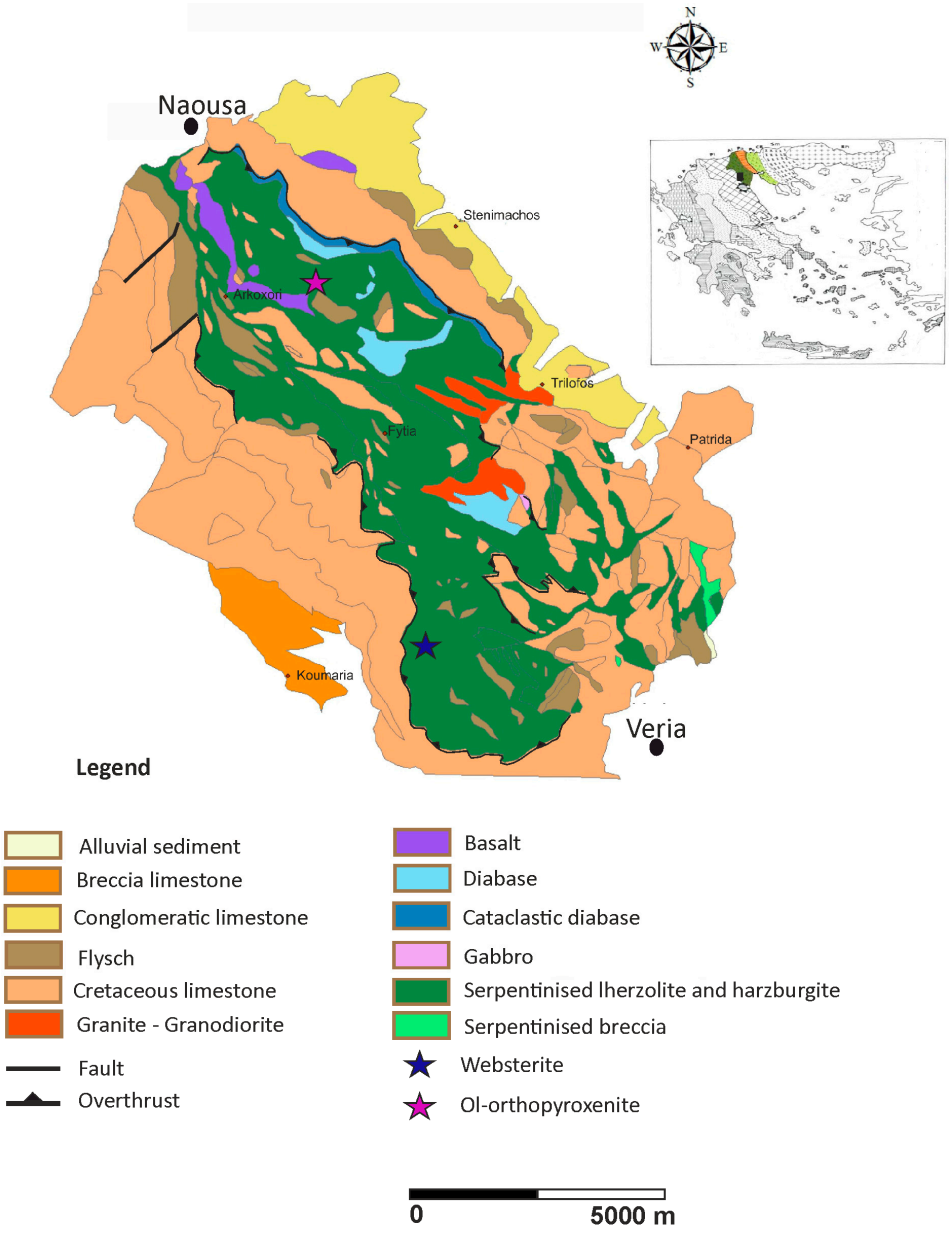

Figure 1. Geological map of the Veria-Naousa region. Inset shows the geotectonic zones of Greece highlighting the Almopias, Paikon and Peonias (from west to east) subzones of the Axios zone; black rectangle shows the study area.

3. Petrographic Features

Pyroxenites show variable degrees of alteration and include two lithotypes: websterite and Ol-orthopyroxenite.

3.1. Websterite

The websterite presents generally porphyroclastic texture in places obliterated by secondary minerals. It consists of porphyroclasts of orthopyroxene and clinopyroxene, which are surrounded by neoblasts of orthopyroxene and clinopyroxene (Figure 2a,b). Overall, orthopyroxene (50–70 vol. %), clinopyroxene (20–40 vol. %), as well as minor olivine (<5 to 10 vol. %) percentages allow its classification as websterite. Blebs and exsolution lamellae of clinopyroxene are observed in orthopyroxene porphyroclasts. The clinopyroxene occurs either as subhedral tabular grains exhibiting

sub-grain boundaries with orthopyroxene or as neoblasts at the rims of the subhedral clinopyroxene (Figure 2a,b). Olivine generally occurs in the form of subhedral crystals. Variable amounts of secondary serpentine, Cr-bearing chlorite, talc and Cr-magnetite were formed after orthopyroxene, olivine and presumably spinel, during subsequent hydrothermal alteration (Figure 2b). Numerous serpentine veins are observed within cracks and along grain boundaries of olivine, orthopyroxene and clinopyroxene. In places, metasomatic garnet (Ti-andradite), clinopyroxene and rare magnetite developed in veins crosscutting the rock.

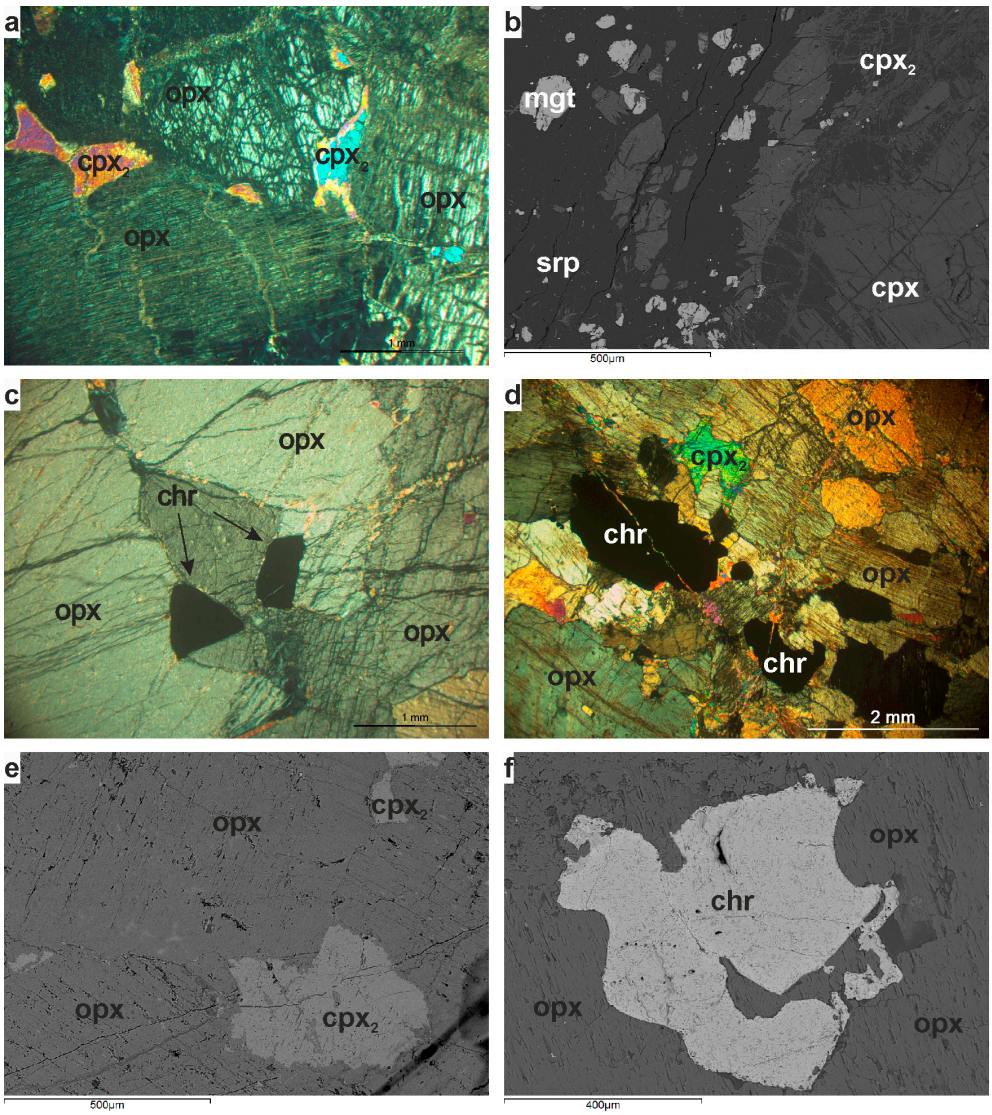

Figure 2. Textural characteristics of the pyroxenites from the Veria-Naousa ophiolite: (**a**) photomicrograph of porphyroclastic orthopyroxene (opx) with lesser clinopyroxene neoblasts (cpx_2) with irregular shapes in a websterite (sample BE.6; Nicols +); (**b**) backscattered electron image of subhedral clinopyroxene (cpx) surrounded by neoblastic clinopyroxene (cpx_2), as well as secondary serpentine (srp) and magnetite (mgt) in a websterite (sample BE.6; Nicols +); (**c**) photomicrograph of porphyroclastic orthopyroxene (opx) and subhedral grains of chromite (chr) in an Ol-orthopyroxenite (sample BE.28); (**d**) photomicrograph of porphyroclastic orthopyroxene (opx) with neoblasts of clinopyroxene (cpx_2) and chromite both subhedral and embayed (chr) in an Ol-orthopyroxenite (sample BE.67B, Nicols +); (**e**) backscattered electron image of clinopyroxene neoblasts (cpx_2) in orthopyroxene (opx) in an Ol-orthopyroxenite (sample BE.67); and (**f**) backscattered electron image of a chromite (chr) with lobate boundaries surrounded by orthopyroxene in an Ol-orthopyroxenite (sample BE.67B).

3.2. Ol-Orthopyroxenite

The Ol-orthopyroxenite samples generally display a porphyroclastic texture and their primary modal mineralogical composition includes orthopyroxene (70–80 vol. %), clinopyroxene (up to 5 vol. %), olivine (~10 vol. %) and Cr-spinel (5–10 vol. %) (Figure 2c,d). Rare Fe-Ni-Co sulphides coexist with Cr-spinel. Orthopyroxene porphyroclasts (up to 2 cm long, Figure 2d) exhibit local kink bands, undulatory extinction and frequent exsolution lamellae of clinopyroxene. Unstrained smaller orthopyroxene and lesser clinopyroxene comprise a younger generation and are dispersed along rims or enclosed in orthopyroxene porphyroclasts (Figure 2e). Two generations of Cr-spinel grains occur: The first includes subhedral to anhedral magnesiochromites to chromites commonly with lobate boundaries (Figure 2d,f). Infrequently, they form kelyphitic textures surrounded by orthopyroxene or, more often, they occur along orthopyroxene grain boundaries. The second includes smaller subhedral (rarely euhedral) magnesiochromite to chromite crystals (Figure 2c,d). Serpentine is the dominant alteration product forming mesh and bastite textures; lesser amounts of chlorite, talc and magnetite occur, as well.

4. Analytical Methods

The mineralogical and textural characteristics of the samples were studied in polished-thin sections in polarising optical and scanning electron microscopes (SEM). Mineral microanalyses were performed using a JEOL JSM-6300 SEM equipped with energy dispersive and wavelength spectrometers (EDS and WDS) and INCA software at the Laboratory of Electron Microscopy and Microanalysis, University of Patras, Greece. Operating conditions were accelerating voltage 25 kV and beam current 3.3 nA, with a 4-μm beam diameter. The total counting time was 60 s and dead-time 40%. Synthetic oxides and natural minerals were utilised as standards for our analyses. Detection limits are ~0.01% and accuracy better than 5% was obtained. Whole-rock chemical analyses for major and trace elements were performed at Bureau Veritas Mineral Laboratories, Vancouver, Canada. Major element analyses were carried out using an XRF spectrometer and a sequential spectrometer (ICP-ES). Trace elements and rare earth elements were determined on totally digested samples by inductively coupled plasma-mass spectrometry (ICP-MS) in the same laboratory. Detection limits for major and trace elements range from 0.01 wt % to 0.04 wt % and from 0.01 ppm to 10 ppm, respectively. The analytical precision calculated from replicate analyses is better than 3% for most major elements and better than 5% for trace elements.

5. Mineral Chemistry

5.1. Orthopyroxene

Orthopyroxene crystals in the analysed Ol-orthopyroxenite and websterite are enstatites with relatively homogenous compositions (Table 1). The Mg# (= 100 × Mg/(Mg + Fe^{2+}) in atoms per formula unit) of the orthopyroxenes in the Ol-orthopyroxenite is lower (87.1–91.4) than the Mg# of the orthopyroxenes in the websterite (90.5–92.5) (Figure 3a,b). The porphyroclastic enstatites in the Ol-orthopyroxenite and websterite are generally richer in Al (with large overlap) and poorer in Ca and Cr than the secondary enstatites (Figure 3a,b). Overall, the enstatites of the websterite have higher amounts of Al_2O_3 (1.90–3.15 wt %) and lower FeO contents (4.84–6.17 wt %) than those in the Ol-orthopyroxenite (0.28–2.03 wt % and 5.47–8.20 wt %, respectively) (Figure 3b). All orthopyroxenes have low CaO (<3 wt %) and Cr_2O_3 (<0.95 wt %).

5.2. Clinopyroxene

Representative clinopyroxene analyses from the investigated websterite and Ol-orthopyroxenite are listed in Table 2. They comprise diopsides with low Al_2O_3, Cr_2O_3 and particularly TiO_2 contents (Figure 3c,d). The neoblastic and the porphyroclastic diopsides in these pyroxenites form two geochemically distinct groups. The porphyroclastic diopsides display lower contents in Ca and

Fe, and higher contents in Al, and Cr, Mg and Mg# (Mg# is particularly true for the websterite only) having mantle affinities (Figure 3c,d). Some clinopyroxene neoblasts show slight enrichments in Mn.

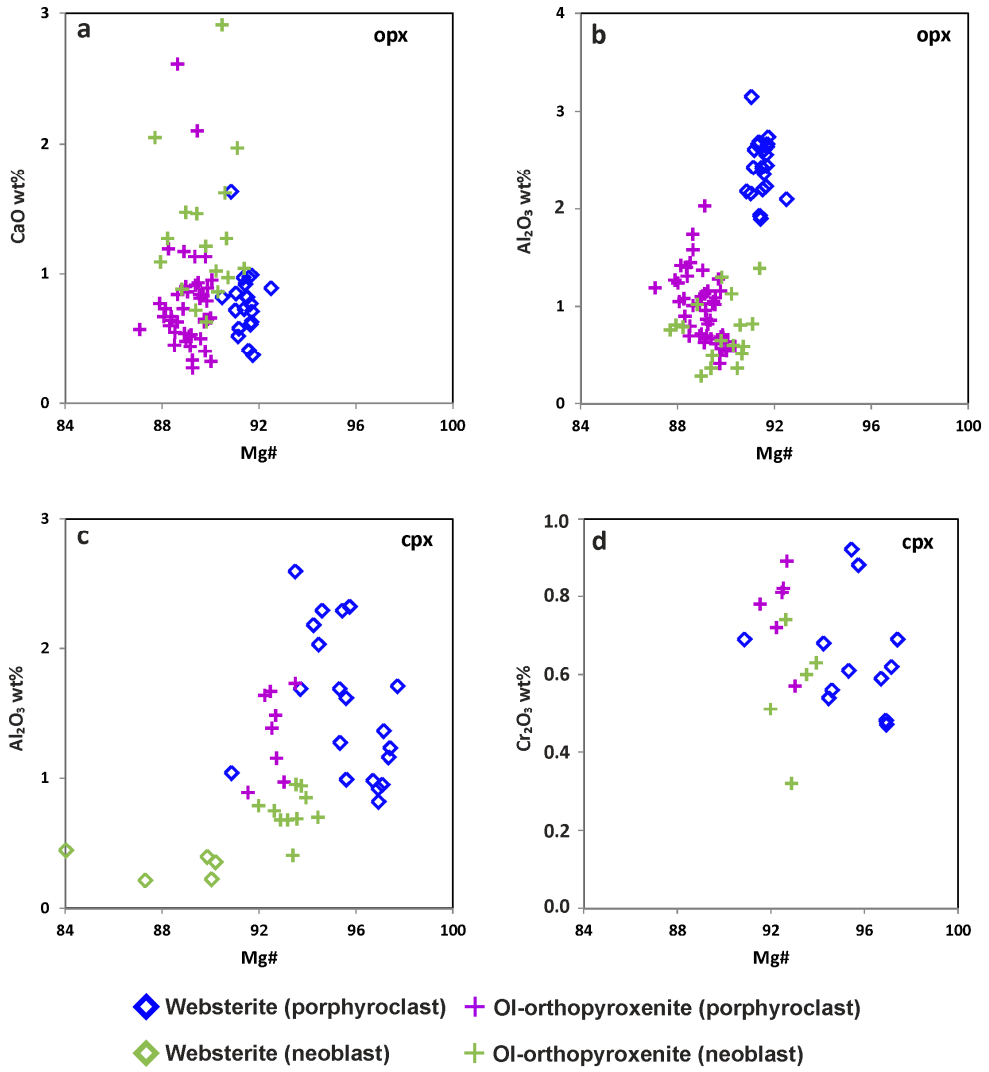

Figure 3. Orthopyroxene and clinopyroxene compositions of the Veria-Naousa pyroxenites: (**a**) CaO vs. Mg# in orthopyroxene; (**b**) Al_2O_3 vs. Mg# in orthopyroxene; (**c**) Al_2O_3 vs. Mg# in clinopyroxene and (**d**) Cr_2O_3 vs. Mg# in clinopyroxene.

5.3. Olivine

Representative olivine analyses from the Ol-orthopyroxenite are listed in Table 3. Fo contents range from 88.9 to 89.6, which are similar to Fo values of olivines from typical supra-subduction zone (SSZ) peridotites (Fo = 87–94 [38]). We were unable to obtain reliable microanalyses from the websterite due to extensive serpentinisation. The analysed olivines show a rather uniform composition, having in particular, very similar FeO (9.75–10.46 wt %) and MgO (46.22–49.10 wt %) contents. NiO contents are rather high ranging from 0.22 to 0.46 wt %, in the range of average NiO concentrations for mantle olivines (0.25–0.51 wt % [39]).

5.4. Spinel-group Minerals

Representative analyses of spinel-group minerals are reported in Table 4 and plotted in Figure 4. Anhedral and subhedral to euhedral crystals comprise two texturally different generations of spinels in the Ol-orthopyroxenite. Both are magnesiochromites to chromites and show similar ranges of

Mg# (28.1–54.4) and Cr# (= 100 × Cr/(Cr + Al), atomic ratios, 52.5–86.9). A number of analyses from both generations cluster in the field of spinels occurring in boninitic basalts, whereas some others are plotted mostly in the field of spinels from marginal basins basalts (Figure 4).

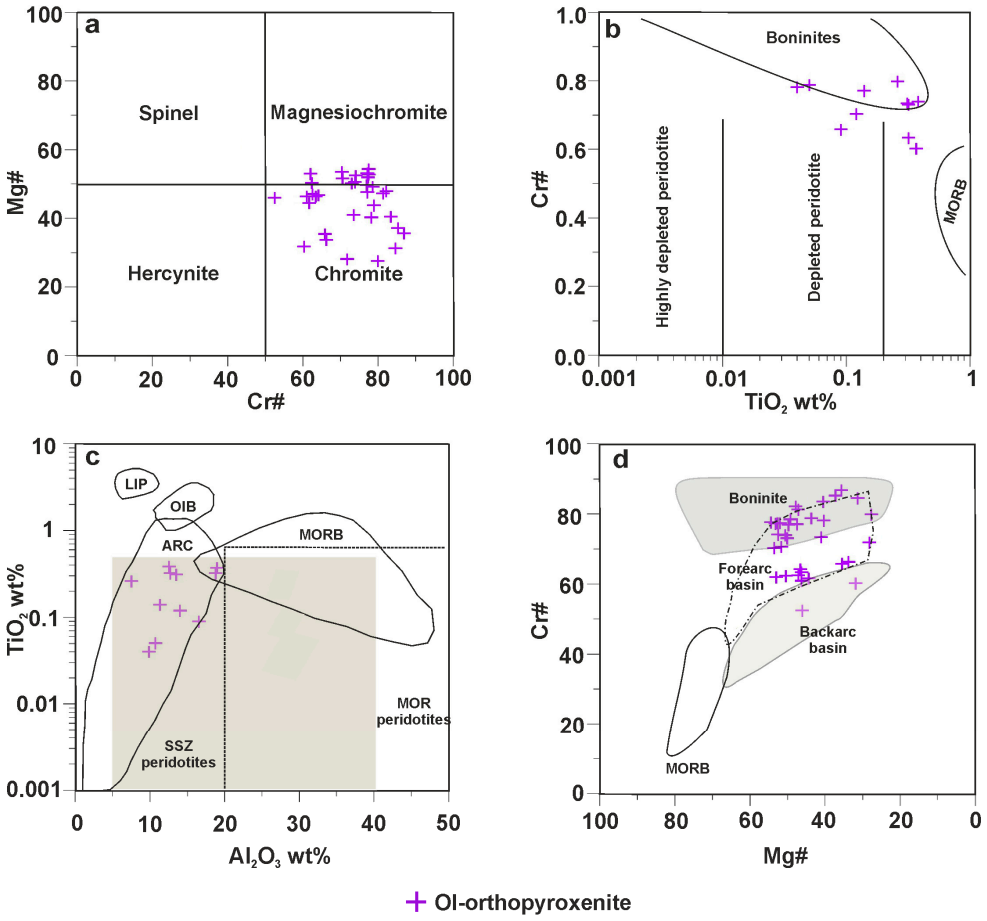

Figure 4. Compositional variations of the spinel-group minerals from the Ol-orthopyroxenites of the Veria-Naousa ophiolite: (**a**) Cr# vs. Mg# chemical classification diagram; (**b**) TiO_2 vs. Cr# diagram [40–42]; (**c**) Al_2O_3 vs. TiO_2 diagram [43]; and (**d**) Mg# vs. Cr# diagram (boninite field after [32], MORB, forearc basin and backarc basin fields after [40]).

6. Whole-Rock Geochemistry

Major, trace and rare earth elements data from the pyroxenites from the Veria-Naousa ophiolite are listed in Table 5 and their compositional variations are illustrated in Figures 5–7. One websterite and three Ol-orthopyroxenite samples were analysed. Care was taken in screening the samples for whole-rock analyses, as well as for the interpretations, as variable degrees of serpentinisation are observed in the pyroxenites, therefore only the freshest samples have been considered. The websterite has higher loss on ignition (LOI) (8.8 wt %) than the other orthopyroxenites (1.1–2.9 wt %) as a result of its higher degree of alteration.

On a volatile-free basis, the Ol-orthopyroxenite samples are richer in SiO_2 (Figure 5a) than the websterite and are silica-hypersthene normative, as an indication for their chemical modification by silica rich fluids. They show moderate Mg# ranging from 80.1 to 81.7 (Table 5). On a volatile-free basis, the websterite is poor in Fe_2O_3 but it contains higher Al_2O_3 and expectedly higher CaO than the Ol-orthopyroxenite (Figure 5b,c). It also shows the highest CaO/Al_2O_3 ratio (Figure 5d) and Mg# (87.9) and has an olivine-hypersthene normative composition.

All samples are poor in incompatible high field strength elements (HFSE) but, generally, the websterite is the most depleted of all (Table 5). Ni contents vary strongly with the Ol-orthopyroxenites having the lowest Ni values (81.3−655.0, Figure 6b, Table 5). The analysed pyroxenites from Veria-Naousa show considerable geochemical similarities in terms of major and some compatible and incompatible trace elements to pyroxenites from Cabo Ortegal (Figures 5 and 6). The websterite and the Ol-orthopyroxenite are strongly depleted in REE, with many REE values below detection limits. LREE in the websterite lie below their detection limits hence a general positive fractionated REE normalised pattern can be inferred for this sample (Figure 7). The Ol-orthopyroxenites are strongly depleted in middle REE showing enrichments in both LREE and HREE, resembling rocks with concave upwards REE normalised patterns (Figure 7). These LREE enriched patterns are similar to most of the well-known pyroxenite assemblages which show depletions in LREE relative to HREE [27,45], and show considerable similarities to pyroxenites from Cabo Ortegal.

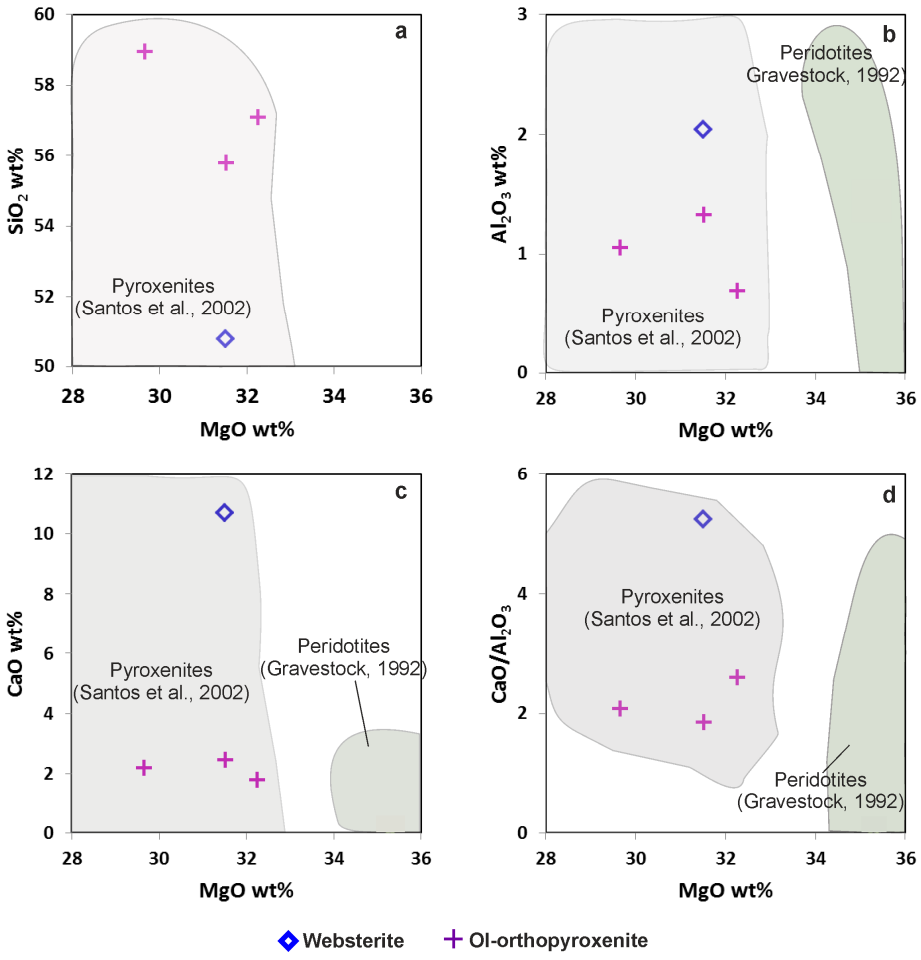

Figure 5. Variations of MgO versus: SiO_2 (**a**); Al_2O_3 (**b**); CaO (**c**); and CaO/Al_2O_3 (**d**), for the pyroxenites from the Veria-Naousa ophiolite (recalculated values to 100% on an anhydrous basis). Fields include data from Gravestock [44] and Santos et al. [45] for the Cabo Ortegal pyroxenites and peridotites.

Table 1. Representative electron microanalyses of orthopyroxenes from the Veria-Naousa pyroxenites (Porph.: porphyroclast, Neobl.: neoblast, -: below detection limit).

Sample	BE.6-2	BE.6-7	BE.28-2	BE.28-4	BE.67-3	BE.67-17	BE.67-32	BE.67B-5	BE.67B-6	BE.67B-8	BE.67B-14
Rock-Type (wt %)	**Webst. Porph.**	**Webst. Porph.**	**Ol-Orthop. Porph.**	**Ol-Orthop. Porph.**	**Ol-Orthop. Porph.**	**Ol-Orthop. Porph.**	**Ol-Orthop. Neobl.**	**Ol-Orthop. Neobl.**	**Ol-Orthop. Neobl.**	**Ol-Orthop. Porph.**	**Ol-Orthop. Porph.**
SiO_2	57.38	57.23	57.86	58.52	58.14	57.18	54.69	56.86	58.15	56.69	56.99
TiO_2	-	-	-	-	-	-	-	-	-	-	-
Al_2O_3	2.18	2.61	0.51	0.41	0.87	0.79	0.76	0.82	0.81	0.81	1.40
FeO	5.87	5.45	6.10	6.63	7.18	7.73	9.07	5.54	5.95	7.37	7.38
MnO	-	-	-	0.23	-	-	-	-	-	0.38	0.34
MgO	32.71	33.26	33.21	33.71	33.25	32.51	32.66	31.85	32.16	31.72	32.94
CaO	1.63	0.97	1.27	0.50	0.91	1.27	2.05	1.97	1.62	1.09	0.48
Cr_2O_3	-	-	-	0.29	-	-	-	0.45	0.45	0.29	0.40
Sum	99.77	99.52	98.95	100.29	100.40	99.48	98.32	97.49	99.14	98.35	99.93
Structural formula units based on 6 oxygens											
Si	1.978	1.971	1.999	1.999	2.000	1.994	1.931	2.000	2.000	2.000	1.976
Al^{iv}	0.022	0.029	0.001	0.001	0.000	0.006	0.000	0.000	0.000	0.000	0.024
Al^{vi}	0.067	0.076	0.032	0.027	0.036	0.027	0.032	0.042	0.051	0.033	0.034
Fe^{3+}	0.000	0.000	0.000	0.000	0.000	0.000	0.107	0.000	0.000	0.000	0.000
Ti	0.000	0.000	0.000	0.000	0.000	0.000	0.000	0.000	0.000	0.000	0.000
Cr	0.000	0.000	0.000	0.008	0.000	0.000	0.000	0.013	0.012	0.008	0.011
Mg	1.681	1.707	1.721	1.727	1.706	1.690	1.719	1.677	1.664	1.668	1.703
Fe^{2+}	0.169	0.157	0.177	0.190	0.207	0.225	0.134	0.164	0.173	0.217	0.214
Mn	0.000	0.000	0.000	0.007	0.000	0.000	0.000	0.000	0.000	0.011	0.010
Ca	0.060	0.036	0.047	0.018	0.034	0.047	0.078	0.075	0.060	0.041	0.018
En	88.0	89.9	88.5	88.9	87.7	86.1	84.4	87.6	87.7	86.1	87.6
Fs	8.9	8.3	9.1	10.2	10.6	11.5	11.8	8.5	9.1	11.8	11.5
Wo	3.2	1.9	2.4	0.9	1.7	2.4	3.8	3.9	3.2	2.1	0.9
Mg#	90.9	91.6	90.7	90.1	89.2	88.2	87.7	91.1	90.6	88.5	88.8

Table 2. Representative electron microanalyses of clinopyroxenes from the Veria-Naousa pyroxenites (Porph.: porphyroclast, Neobl.: neoblast, -: below detection limit).

Sample	**BE.6-12**	**BE6-13**	**BE.6-27**	**BE.6-58**	**BE.28-12**	**BE.28-13**	**BE.67-28**	**BE.67-21**	**BE.67B-1**	**BE.67B-4**	**BE.67B-9**
Rock-Type (wt %)	**Webst. Neobl.**	**Webst. Neobl.**	**Webst. Porph.**	**Webst. Porph.**	**Ol-Orthop. Porph.**	**Ol-Orthop. Porph.**	**Ol-Orthop. Porph.**	**Ol-Orthop. Neobl.**	**Ol-Orthop. Neobl.**	**Ol-Orthop. Neobl.**	**Ol-Orthop. Neobl.**
SiO_2	53.41	54.51	53.89	55.07	54.66	55.24	55.23	55.47	53.91	54.53	53.84
TiO_2	-	-	-	-	-	-	-	-	-	-	0.21
Al_2O_3	1.04	0.87	1.27	1.69	0.95	0.75	0.94	0.97	1.02	0.79	0.68
FeO	3.25	3.25	1.98	2.11	2.14	2.47	2.10	2.31	2.41	2.60	2.35
MnO	-	-	-	-	-	-	-	-	0.03	0.25	0.08
MgO	18.14	17.75	22.76	24.13	17.35	17.44	17.68	17.31	17.48	18.37	17.82
CaO	21.98	20.95	18.07	16.85	22.33	22.82	21.96	22.49	22.61	21.36	21.75
Cr_2O_3	0.69	0.77	-	0.61	0.60	0.74	-	0.57	0.49	0.51	0.32
Sum	98.51	98.10	97.97	100.50	98.03	99.46	97.91	99.12	97.95	98.41	97.05
Structural formula units based on 6 oxygens											
Si	1.969	2.000	1.954	1.944	2.000	1.999	2.000	2.000	1.990	1.998	2.000
Al^{iv}	0.031	0.000	0.046	0.056	0.000	0.001	0.000	0.000	0.010	0.002	0.000
Al^{vi}	0.014	0.038	0.008	0.014	0.050	0.038	0.064	0.057	0.035	0.033	0.030
Fe^{3+}	0.000	0.000	0.038	0.025	0.000	0.000	0.000	0.000	0.000	0.000	0.000
Ti	0.000	0.000	0.000	0.000	0.000	0.000	0.000	0.000	0.000	0.000	0.006
Cr	0.020	0.022	0.000	0.017	0.017	0.021	0.000	0.016	0.014	0.015	0.009
Mg	0.997	0.973	1.230	1.270	0.950	0.944	0.966	0.937	0.962	1.004	0.987
Fe^{2+}	0.100	0.100	0.022	0.037	0.066	0.075	0.064	0.070	0.074	0.080	0.073
Mn	0.000	0.000	0.000	0.000	0.000	0.000	0.000	0.000	0.001	0.008	0.003
Ca	0.868	0.826	0.702	0.637	0.879	0.888	0.862	0.875	0.894	0.839	0.866
En	50.7	51.3	61.8	64.5	50.1	49.5	51.0	49.8	49.8	52.0	51.2
Fs	5.1	5.3	3.0	3.2	3.5	3.9	3.4	3.7	3.9	4.5	3.9
Wo	44.2	43.5	35.2	32.4	46.4	46.6	45.6	46.5	46.3	43.5	44.9
Mg#	90.9	90.7	95.3	95.3	93.5	92.6	93.8	93.0	92.7	92.0	92.9

Table 3. Representative electron microanalyses of olivines from Veria-Naousa Ol-orthopyroxenite (-: below detection limit).

Sample	**BE.28-2**	**BE.28-5**	**BE.28-6**	**BE.28-7**	**BE.28-8**	**BE.28-9**
Rock-Type (wt %)	**Ol-Orthop.**	**Ol-Orthop.**	**Ol-Orthop.**	**Ol-Orthop.**	**Ol-Orthop.**	**Ol-Orthop.**
SiO_2	41.55	42.73	42.55	41.34	42.62	41.40
TiO_2	-	-	-	-	-	-
Al_2O_3	-	-	-	-	-	-
FeO	9.75	10.46	10.19	10.19	10.45	10.31
MnO	-	-	-	-	-	-
MgO	46.93	49.10	48.31	46.53	47.62	46.22
CaO	-	-	-	-	-	-
Cr_2O_3	-	-	-	-	-	-
NiO	0.46	0.42	0.43	0.25	0.22	0.49
Sum	98.69	102.71	101.48	98.31	100.91	98.42
Structural formula units based on 4 oxygens						
Si	1.029	1.019	1.025	1.029	1.032	1.030
Al	0.000	0.000	0.000	0.000	0.000	0.000
Ti	0.000	0.000	0.000	0.000	0.000	0.000
Mg	1.732	1.745	1.736	1.726	1.719	1.715
Fe^{2+}	0.202	0.209	0.205	0.212	0.212	0.215
Mn	0.000	0.000	0.000	0.000	0.000	0.000
Ca	0.000	0.000	0.000	0.000	0.000	0.000
Ni	0.009	0.008	0.008	0.005	0.004	0.010
Total	2.970	2.980	2.970	2.970	2.970	2.970
Fo	89.6	89.3	89.4	89.1	89.0	88.9
Fa	10.4	10.7	10.6	10.9	11.0	11.1

Table 4. Representative electron microanalyses of spinel-group minerals from the Veria-Naousa Ol-orthopyroxenite (-: below detection limit).

Sample	**BE.28-2**	**BE.28-3**	**BE.28-4**	**BE.28-5**	**BE.28-6**	**BE.67B-9**	**BE.67B-14**
Rock-Type (wt %)	**Ol-Orthop. Chr**	**Ol-Orthop. Chr**	**Ol-Orthop. Chr**	**Ol-Orthop. Chr**	**Ol-Orthop. Chr**	**Ol-Orthop. Chr**	**Ol-Orthop. Cr-sp**
TiO_2	-	-	-	-	-	0.05	-
Al_2O_3	8.98	9.28	11.64	11.38	11.59	10.70	20.00
FeO	19.77	20.06	19.61	19.47	19.52	21.63	20.59
MnO	0.44	-	-	-	-	0.46	-
MgO	9.57	9.41	10.11	10.84	10.77	8.72	11.49
K_2O	-	-	-	-	-	0.12	-
Cr_2O_3	61.67	60.09	57.89	57.46	58.97	59.47	48.72
NiO	-	-	-	-	-	-	0.18
ZnO	-	-	-	-	-	-	0.19
Sum	100.43	98.84	99.25	99.15	100.85	101.15	101.17
Structural formula units based on 3 cations							
Al	0.351	0.368	0.452	0.441	0.442	0.410	0.731
Cr	1.616	1.597	1.510	1.493	1.509	1.545	1.195
Fe^{3+}	0.033	0.035	0.038	0.066	0.048	0.043	0.074
Ti	0.000	0.000	0.000	0.000	0.000	0.001	0.000
	2.000	2.000	2.000	2.000	2.000	2.000	2.000
Mg	0.473	0.472	0.497	0.531	0.520	0.427	0.531
Ni	0.000	0.000	0.000	0.000	0.000	0.000	0.004
Fe^{2+}	0.515	0.528	0.503	0.469	0.480	0.555	0.460
Mn	0.012	0.000	0.000	0.000	0.000	0.013	0.000
Zn	0.000	0.000	0.000	0.000	0.000	0.000	0.004
K	0.000	0.000	0.000	0.000	0.000	0.005	0.000
	1.000	1.000	1.000	1.000	1.000	1.000	1.000
Cr#	82.2	81.3	76.9	77.2	77.3	78.9	62.0
Mg#	47.9	47.2	49.7	53.1	52.0	43.7	53.6

Table 5. Representative geochemical analyses of pyroxenites from Veria-Naousa ophiolite (-: below detection limit).

Sample	BE.6	BE.28	BE.67	BE.67B
Rock-Type	**Websterite**	**Ol-orthopyroxenites**		
Major Elements (wt %)				
SiO_2	45.76	54.79	57.65	54.79
TiO_2	0.01	-	0.02	0.02
Al_2O_3	1.84	0.66	1.03	1.30
$Fe_2O_3{}^t$	4.34	7.69	7.78	8.57
MnO	0.14	0.16	0.17	0.18
MgO	28.39	30.96	29.01	30.97
CaO	9.64	1.71	2.14	2.40
Na_2O	-	-	0.02	-
K_2O	-	-	-	-
P_2O_5	-	-	-	-
LOI	8.8	2.9	1.2	1.1
Total	98.92	98.87	99.02	99.33
Trace Elements (ppm)				
Cr	2812	3188	2901	3147
Co	66.7	75.4	66.4	69.8
Ni	1563.4	268.4	81.3	655.0
Cu	23.9	3.2	3.9	5.4
Zn	22	10	6	5
Rb	0.5	2.5	1.7	1.4
Sr	7.7	19.6	4.2	2.6
Y	0.4	0.3	0.3	0.2
Zr	0.1	0.3	0.5	0.4
Nb	0.1	-	-	2.1
Pb	8.9	6.1	1.5	0.2
Ba	4	5	3	2
V	108	45	92	132
Sc	20	13	21	29
Ga	3.2	3.2	1.3	0.6
Hf	-	-	-	-
As	-	0.6	-	-
Hg	-	0.01	0.02	-
Ta	-	-	-	-
Th	-	-	-	-
U	-	-	-	-
Be	-	2	-	-
Au (ppb)	2.3	3.3	2.2	-
Rare Earth Elements (ppm)				
La	-	0.5	0.7	0.4
Ce	-	0.3	0.3	0.2
Pr	-	0.02	0.03	-
Nd	-	-	-	-
Sm	-	-	-	-
Eu	-	-	-	-
Gd	0.05	-	-	-
Tb	-	-	-	-
Dy	-	-	-	0.09
Ho	-	-	-	-
Er	0.06	0.03	0.03	0.06
Tm	0.01	-	-	-
Yb	0.09	0.07	0.06	0.06
Lu	0.02	-	0.02	0.01
Mg#	87.9	81.7	80.6	80.1
CaO/Al_2O_3	5.24	2.59	2.08	1.85
Zr/Y	0.25	1.00	1.67	2.00
La/Lu	-	7.14	11.67	6.67

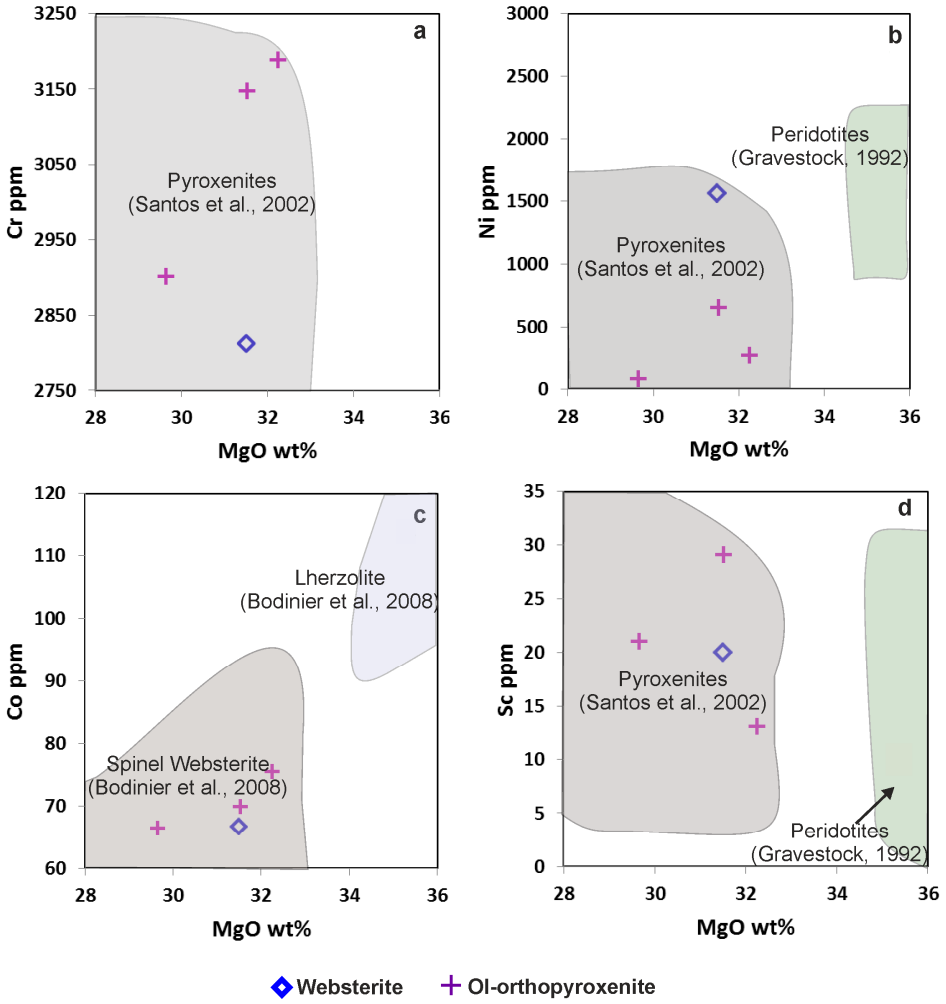

Figure 6. Variations of MgO versus: Cr (**a**); Ni (**b**); Co (**c**); and Sc (**d**), for the pyroxenites from the Veria-Naousa ophiolite (recalculated values to 100% on an anhydrous basis). Fields include data from Gravestock [44] and Santos et al. [45] for the Cabo Ortegal pyroxenites and peridotites, Bodinier et al. [11] for the Ronda spinel websterite and lherzolite.

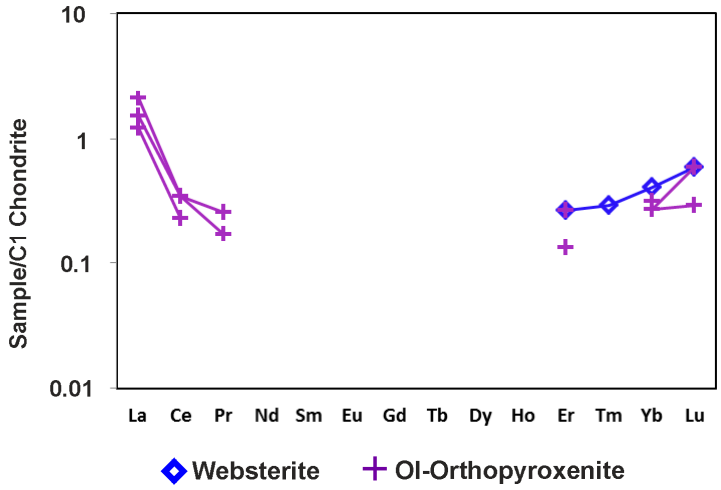

Figure 7. Chondrite-normalized REE patterns of the analysed pyroxenites. Normalising values are after [46].

7. Geothermometry

The equilibration temperatures for websterite and Ol-orthopyroxenite were determined using two-pyroxenes (clinopyroxene-orthopyroxene) thermometry proposed by Wood and Banno [47]. Rim composition of the coexisting mineral pairs has been used for geothermometry calculation. We selected co-existing mineral phases for estimation of temperature. These co-magmatic mineral phases have a well-defined common boundary with no evidence of alteration and similar Mg#, which indicate that they have attained the equilibrium condition.

Two-pyroxene thermometry indicates equilibration temperature of 1136 °C for the websterite and 972–974 °C for Ol-orthopyroxenites (Table 6).

Table 6. Temperature (T °C) estimates on pyroxenites from the Veria-Naousa ophiolite.

Sample	BE.6	BE.28	BE.67	BE.67B
Rock-Type	Websterite	Ol-orthopyroxenite		
Opx-Cpx thermometry (°C) Wood and Bano [47]	1136	972	974	974

8. Petrogenetic and Geodynamic Considerations

8.1. Origin of Ol-Orthopyroxenite and Websterite

Several lines of evidence suggest that the Ol-orthopyroxenite and the websterite are results of melt-rock reaction. The occurrence of porphyroclasts of orthopyroxene and olivine with mantle affinities in the pyroxenites suggests mantle peridotite precursors. Their highly depleted nature in HFSE and the high Cr (and Ni in the websterite) contents strongly suggest a residual character for their precursors, which must have been affected by plastic asthenospheric deformation. Spinel with lobate boundaries is compatible with a dominant partial melting process, which is normally observed in such residual peridotites. A harzburgite precursor appears most probable for the Ol-orthopyroxenite whereas a residual lherzolite is more likely the precursor of the websterite, as inferred from the presence of abundant diopsidic porphyroclast relics. This evidence is compatible with the host rocks of the collected lithotypes. Microtextures, like interstitial orthopyroxene and clinopyroxene, as well as subhedral to euhedral Cr-spinels are commonly related to melt-rock reactions and refertilisation [48,49]. Such a formation of orthopyroxene and clinopyroxene neoblasts involves two possible reactions, which can describe the formation of the Ol-orthopyroxenite and the websterite, respectively:

$$\text{forsterite} + \text{Si-rich melt} \rightarrow \text{enstatite} + \text{Si-poorer melt} \quad (1)$$

$$\text{forsterite} + \text{melt 1} \rightarrow \text{enstatite} + \text{diopside} + \text{melt 2} \quad (2)$$

The above reactions commonly involve the formation of an Al-rich phase, which, in the case of the Veria-Naousa pyroxenites, is spinel and have been described in Archean cratons [29,50] or subcontinental mantle regions such as the Lherz Mountains [51], Ronda [11,52,53] and Cabo Ortegal [45,54]. However, quite recently, it was documented that such reactions producing two pyroxenes after dissolution of olivine can also occur in abyssal pyroxenites [55]. Quantification of the melt/rock ratio is a complicated task that involves a number of parameters, such as changes in modal abundances and the trace element compositions of minerals and can be obtained with confidence if an adequate number of samples is available. In the limited samples available in the Veria-Naousa region, we can only provide qualitative estimations and we interpret that the rather rich in olivine Ol-orthopyroxenites indicate a moderate melt/rock ratio whereas the websterite with limited olivine suggest a higher melt/rock ratio, which is compatible with the much higher CaO/Al_2O_3 ratio in the websterite.

Reaction (1), which causes Si metasomatism, frequently occurs in the mantle wedge. Natural and experimental data reveal that Si-rich melts [56,57], or aqueous [58] or supercritical fluids [59]

are released from the underlying subducted oceanic slab into the sub-arc region driving the dissolution of mantle olivine and the neoformation of pyroxenes and Al-phases in a range of pressures between 0.8 and 3.4 GPa [60–68]. Experimental results of Grant et al. [69] at 800 MPa suggest that neoblasts of orthopyroxene and clinopyroxene form at a relatively narrow temperature range of around 800 to 900 °C (with few exceptions up to 1100 °C). Topological conditions like the existence of veins and the SSZ geotectonic environment proposed below (see Section 8.2) render the conditions of the studied Veria-Naousa ophiolite comparable to those of Grant et al. [69] and hence, our geothermometric calculations for the Ol-orthopyroxenites are consistent with the calculated temperatures of these authors.

The metasomatic orthopyroxene and clinopyroxene are generally poorer in Al, but richer in Ca relative to porphyroclasts whereas the metasomatic orthopyroxenes are richer in Cr relative to the porphyroclasts in both rock-types. This behaviour of Ca and Cr is not in agreement with other natural examples [61,70,71] and may imply percolation of a melt that was richer in Ca and Cr than the pyroxenite's precursors. Relic crystals with lobate boundaries and newly-formed, euhedral spinel crystals in Ol-orthopyroxenite show a range of Cr# resembling spinels from both marginal basins and boninitic basalts (Figure 4b–d). This evidence implies that apart from the crystallisation of spinels with boninitic affinities, residual mantle spinels have also been modified by impregnation from a boninitic melt. The mechanisms for formation and transformation of spinels in the upper mantle through a necessary peridotite-melt reaction process were recently reviewed by Arai and Miura [72]. The elevated Mg# of these rocks, as well as their high Cr and low Ti and Al abundances are compatible with an imprint of a boninitic geochemical signature. This hypothesis is in agreement with the enrichments in LREE and HREE in the REE patterns of the Ol-orthopyroxenites, as boninitic melts, which are typically known to fractionate MREE, may have imprinted their REE signature on the investigated rocks (Figure 7). Similar U-shaped REE patterns have been reported and modelled describing the nature of melt/rock interactions in Greek and other ophiolites [73–77]. Several authors have attributed LREE enrichments in ultramafic rocks to secondary events and particularly to serpentinisation (for a review see [78]), however such a hypothesis is less likely, as the Ol-orthopyroxenites are the least altered and no striking LREE enrichments are observed in any of the pyroxenites. The very low Al contents in the neoblastic pyroxenes also support this hypothesis, as experimental data have shown that such crystals form from hydrous melts with a low Al/Si ratio similar to boninites [79].

The websterite is the most LREE depleted pyroxenite showing however HREE contents similar to the Ol-orthopyroxenite. This resemblance points towards a precursor with similar levels of depletion for both rock-types, however the occurrence of clinopyroxene porphyroclasts along with the lower Cr contents in the websterite indicate a more fertile character for its precursor, compatible with its host refractory lherzolite. Both the websterite and Ol-orthopyroxenite show rather elevated CaO/Al_2O_3 ratios (5.24 and 1.85–2.59, respectively) with nevertheless a much higher ratio in the websterite. This is a strong indication for the involvement of higher amounts of percolating magma in their origin. Furthermore, CaO/Al_2O_3 ratios higher than 5 have been assigned to the interaction of peridotites with carbonatite magmas [80], which commonly share their origin with ankaramitic magmas. It is known that boninites and ankaramites have similar origins (both with highly magnesian olivine and Cr-rich spinels) but they differ in that boninites include enstatite or bronzite whereas ankaramites involve the crystallization of diopside [81,82]. Thus, the diopside neoblasts further advocate to the incorporation of ankaramitic melts in the evolution of the websterite. It has been documented that such a process may result in depletions of Zr and reduction of Zr/Y ratios [83–85] similar to the studied websterite, which shows lower Zr and Zr/Y ratio than the Ol-orthopyroxenite (see Table 5). However, no primary carbonates have been observed that would further support this hypothesis. The high Mg# of the neoblastic pyroxenes suggests crystallisation from a nearly primitive magma, which may also account for the whole-rock high Mg# and Ni of the websterite. High pressure (>1.5 GPa) melting of refractory lherzolites or clinopyroxene-bearing harzburgites is required and can be triggered from variations in the CO_2 and H_2O contents in the mantle wedge, which may have been fluxed

from the subducted Pelagonian sediments [86,87], to produce carbonatitic or picritic-ankaramitic melts [88–90]. Ankaramitic melts are highly magnesian as boninites and are produced at around 1300–1350 °C, at 40–70 km depth [90]. The calculated temperature of 1136 °C for the websterite does not contradict such an ascending, percolating melt, which had slightly cooled prior to the interaction with the wall-rock peridotite. Ankaramitic melts are generally enriched in incompatible elements. The low amounts of incompatible elements in the websterite can be explained by the late quantitative imprint by H_2O-rich fluids, which are poor in these elements. This is a common process in subarc mantle, as demonstrated by Green et al. [90]. We recommend that these melts may have subsequently differentiated to the boninitic melts, which impregnated harzburgite, perhaps at a higher level, to form the Ol-orthopyroxenite. This is a process similar to what has been proposed for the pyroxenites of Cabo Ortegal [54].

Koloskov and Zharinov [91] have proposed a multivariate statistical diagram of clinopyroxene compositions in ultramafic and mafic rocks discriminating tectonic zones of clinopyroxenes in equilibrium with garnet (zones I and II), spinel (zones III and IV) and plagioclase (zones V, VI and VII). Despite that the statistical treatment has been questioned by Buccianti and Vaselli [92] other authors have tested the validity and argue for the significance of this diagram, even though a precise setting of different clinopyroxene origins may not be well enough established [45]. The analysed clinopyroxenes from both the Ol-orthopyroxenite and the websterite plot in the field of island arc peridotites (Figure 8) with the first being moreover very similar to clinopyroxenes from the Izu Bonin Marianna forearc peridotites. This is compatible with the replacive character of the Veria-Naousa pyroxenites and their genesis in a mantle wedge or sub-arc setting.

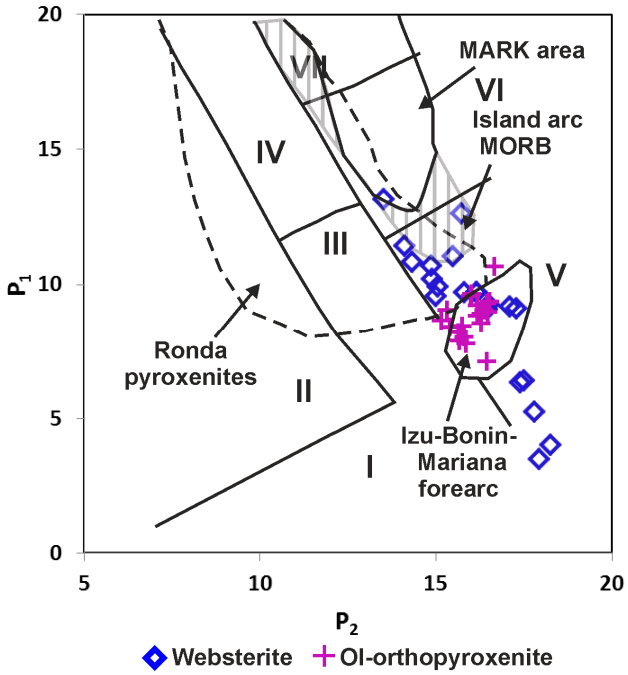

Figure 8. Tectonic discrimination diagram for pyroxenitic clinopyroxenes from the Veria-Naousa ophiolite. Fields I–VII and parameters P_1 and P_2 are as defined Koloskov and Zharinov [91]: $P_1 = -0.02SiO_2 + 0.09TiO_2 + 0.64Al_2O_3 + 0.59Cr_2O_3 + 1.35FeO + 9.65MnO - 0.50MgO + 0.29CaO - 2.26Na_2O + 8.0$; and $P_2 = 0.93TiO_2 + 0.07Al_2O_3 + 1.23Cr_2O_3 - 0.46FeO + 1.74MnO + 0.36MgO + 0.10CaO - 1.66Na_2O + 8.0$. Fields: I, peridotite xenoliths in kimberlites; II, eclogites and pyrope-bearing pyroxenites in kimberlites; III, spinel peridotites; IV, spinel pyroxenites; V, island arc peridotites; VI, island arc pyroxenites; and VII, plagioclase-bearing xenoliths in volcanic rocks from island arcs. Data sources: island arc and mid-ocean ridges [91]; Izu-Bonin-Mariana forearc [93]; Ronda pyroxenites [94]; Mid-Atlantic Ridge Kane Fracture Zone (MARK area [95]).

8.2. Tectonic Setting

Unzoned pyroxenes occur in the pyroxenites from the Veria-Naousa ophiolite, which may indicate slow cooling during crystallisation. It is believed that the slowly cooling, unzoned minerals are indicative of crystallisation in a high-pressure environment [96]. The existence of highly magnesian olivine, pyroxene neoblasts and the absence of plagioclase are in line with high pressure crystallisation of basaltic melts [97]. Al contents of the clinopyroxenes and orthopyroxenes in both lithologies are compatible with formation in a SSZ regime. The compositions of the magnesiochromites-chromites in the Veria-Naousa pyroxenites vary widely in Cr# and Mg#, and have low TiO_2 contents showing affinities similar to boninitic or backarc forming spinels. This evidence is in agreement with the composition of the clinopyroxenes in these pyroxenites that have affinities analogous to crystals from arc peridotites.

The REE patterns of the Ol-orthopyroxenite provide further evidence for their impregnation from boninitic melts (Figure 7). The enriched in Al_2O_3 and relatively poor Mg# nature of the analysed pyroxenes in the Ol-orthopyroxenites can be explained from the influence of metasomatic impregnation from fluids generated in a supra-subduction zone setting (Figure 4a,c) [98]. The low TiO_2 content in the clinopyroxene from websterite and Ol-orthopyroxenite is interpreted as the result of crystallisation from a Ti-poor magma, similar to that typically generated in SSZ settings [6].

9. Conclusions

New occurrences of websterite and Ol-orthopyroxenite have been discovered in the Veria-Naousa ophiolite. The precursor of the websterite is a more fertile clinopyroxene-bearing lherzolite. Geochemical signatures imply that it was formed from the replacement of olivine from two pyroxenes, induced by the channeled flow of a nearly primitive ankaramitic/carbonatitic melt. The Ol-orthopyroxenites are replacive formations after a harzburgitic precursor with the progressive replacement of olivine by orthopyroxene, induced by channelled flow of boninitic melts, perhaps at a higher level than the websterite. The evolution of both the Ol-orthopyroxenite and the websterite is attributed to the mantle wedge of a sub-arc region. We recommend that the occurrence of the pyroxenites record the evolution of the mantle wedge and the opening of a backarc basin in the region of the Axios (Vardar) Ocean in the region of the Veria and Naousa.

Acknowledgments: This work forms part of the PhD study of Aikaterini Rogkala. We thank Cassian Pirard and three anonymous reviewers for their constructive comments, which greatly improved the manuscript. We kindly thank A.K. Seferlis of the Laboratory of Electron Microscopy and Microanalysis, University of Patras for his assistance with the microanalyses and SEM micrographs.

Author Contributions: Aikaterini Rogkala participated in the fieldwork, in the interpretation of the results and wrote the paper; Petros Petrounias participated in the fieldwork, the interpretation of results and performed SEM work; Basilios Tsikouras participated in the fieldwork, the interpretation of the results, coordinated the research and wrote the paper; and Konstantin Hatzipanagiotou participated in the interpretation of results.

Conflicts of Interest: The authors declare no conflict of interest.

References

1. Dilek, Y.; Furnes, H. Ophiolites and Their Origins. *Mineral. Soc. Am.* **2014**, 1811–5209. [CrossRef]
2. Magganas, A.; Koutsovitis, P. Composition, melting and evolution of the upper mantle beneath the Jurassic Pindos ocean inferred by ophiolitic ultramafic rocks in East Othris, Greece. *Int. J. Earth Sci.* **2015**, *104*, 1185–1207. [CrossRef]
3. Ribeiro, A.; Munhá, J.; Fonseca, P.E.; Araújo, A.; Pedro, J.C.; Mateus, A.; Tassinari, C.; Machado, C.; Jesus, A. Variscan ophiolite belts in the Ossa-Morena Zone (Southwest Iberia): Geological characterization and geodynamic significance. *Gondwana Res.* **2010**, *17*, 408–421. [CrossRef]
4. Pearce, J.A.; Robinson, P.T. The Troodos ophiolite complex probably formed in a subduction initiation, slab edge setting. *Gondwana Res.* **2010**, *17*, 60–81. [CrossRef]

5. Chetty, T.R.K.; Yellappa, T.; Nagesh, P.; Mohanty, D.P.; Venkatasivappa, V.; Santosh, M.; Tsunogae, T. Structural anatomy of a dismembered ophiolite suite from Gondwana: The Manamedu complex, Cauvery suture zone, southern India. *J. Asian Earth Sci.* **2011**, *42*, 176–190. [CrossRef]
6. Allahyari, K.; Saccani, E.; Rahimzadeh, B.; Zeda, O. Mineral chemistry and petrology of highly magnesian ultramafic cumulates from the Sarve-Abad (Sawlava) ophiolites (Kurdistan, NW Iran): New evidence for boninitic magmatism in intra-oceanic fore-arc setting in the Neo-Tethys between Arabia and Iran. *J. Asian Earth Sci.* **2014**, *79*, 312–328. [CrossRef]
7. Whattam, S.A.; Stern, R.J. The 'subduction initiation rule': A key for linking ophiolites, intra-oceanic forearcs and subduction. *Contrib. Mineral. Petrol.* **2011**, *162*, 1031–1045. [CrossRef]
8. Rizeli, M.E.; Beyarslan, M.; Wang, K.L.; Bingöl, A.F. Mineral chemistry and petrology of mantle peridotites from the Guleman ophiolite (SE Anatolia, Turkey): Evidence of a forearc setting. *J. Afr. Earth Sci.* **2016**, *123*, 392–402. [CrossRef]
9. Rampone, E.; Hofmann, A.W.; Piccardo, C.B.; Vannucci, R.; Bottazzi, P.; Ottolini, L. Petrology, mineral and isotope geochemistry of the external Liguride peridotites (Northern Apennines, Italy). *J. Petrol.* **2005**, *36*, 81–105. [CrossRef]
10. Schmädicke, E.; Gose, J.; Will, T.M. High-temperature metamorphism of garnet-bearing ultramafic rocks from the Saxonian Granulite Core Complex, Germany. *J. Metamorph. Geol.* **2010**, *28*, 489–508. [CrossRef]
11. Bodinier, J.L.; Garrido, C.J.; Chanefo, I.; Bruguier, O.; Gervilla, F. Origin of Pyroxenite-Peridotite Veined Mantle by Refertilization Reactions: Evidence from the Ronda Peridotite (Southern Spain). *J. Petrol.* **2008**, *49*, 999–1025. [CrossRef]
12. Montanini, A.; Tribuzio, R.; Thirwall, M. Garnet clinopyroxenite layers from the mantle sequences of the Northern Apennine ophiolites (Italy): Evidence for recycling of crustal material. *Earth Planet Sci. Lett.* **2012**, *351–352*, 171–181. [CrossRef]
13. Schmädicke, E.; Okrusch, M.; Will, T. Garnet pyroxenite, eclogite and alkremite xenoliths from the off-craton Gibeon kimberlite field, Namibia: A window into the upper mantle of the Rehoboth Terrane. *Precamb. Res.* **2011**, *191*, 1–17. [CrossRef]
14. Schmädicke, E.; Will, T.; Mezger, K. Garnet pyroxenite from the Shackleton Range, Antarctica: Intrusion of plume-derived picritic melts in the continental lithosphere during Rodinia breakup. *Lithos* **2015**, *238*, 185–206. [CrossRef]
15. Bizimis, M.; Sen, G.; Salters, V.J.M.; Keshav, S. Hf-Nd-Sr isotope systematics of garnet pyroxenites from Salt Lake Crater, Oahu, Hawaii: Evidence for a depleted component in Hawaii volcanism. *Geochim. Cosmochim. Acta* **2005**, *69*, 2629–2646. [CrossRef]
16. Hirschmann, M.M.; Stolper, E.M. A possible role for garnet pyroxenite in the origin of the 'garnet signature' in MORB. *Contrib. Mineral. Petrol.* **1996**, *124*, 185–208. [CrossRef]
17. Hirschmann, M.M.; Kogisto, T.; Baker, M.B.; Stolper, E.M. Alkalic magmas generated by partial melting of garnet pyroxenite. *Geology* **2003**, *31*, 481–483. [CrossRef]
18. Sobolev, A.V.; Hofmann, A.W.; Sobolev, S.V.; Nikogosian, I.K. An olivine-free mantle source of Hawaiian shield basalts. *Nature* **2005**, *434*, 590–597. [CrossRef] [PubMed]
19. Tuff, J.; Takahashi, E.; Gibson, S.A. Experimental constraints on the role of garnet pyroxenite in the genesis of High-Fe mantle plume derived melts. *J. Petrol.* **2005**, *46*, 2023–2058. [CrossRef]
20. Schiano, P.; Eiler, J.M.; Hutcheon, I.D.; Stolper, E.M. Primitive CaO-rich, silica-undersaturated melts in island arcs, evidence for the involvement of clinopyroxene-rich lithologies in the petrogenesis of arc magmas. *Geochem. Geophys. Geosyst.* **2000**, *1*. [CrossRef]
21. Lee, C.T.A.; Cheng, X.; Horodyskyi, U. The development and refinement of continental arcs by primary basaltic magmatism, garnet pyroxenite accumulation, basaltic recharge and delamination: Insights from the Sierra Nevada. *Contrib. Mineral. Petrol.* **2006**, *151*, 222–242. [CrossRef]
22. Esna-Ashari, A.; Tiepolo, M.; Hassanzadeh, J. On the occurrence and implications of Jurassic primary continental boninite-like melts in the Zagros orogeny. *Lithos* **2016**, *258–259*, 37–57. [CrossRef]
23. Herzberg, C. Identification of source lithology in the Hawaiian and Canary Islands: Implications for origins. *J. Petrol.* **2011**, *52*, 113–146. [CrossRef]
24. Frets, E.; Tommasi, A.; Garrido, C.J.; Padrón-Navarta, J.A.; Amri, I.; Targuisti, K. Deformation processes and rheology of pyroxenites under lithospheric mantle conditions. *J. Struct. Geol.* **2012**, *39*, 138–157. [CrossRef]

25. Ying, J.F.; Zhang, H.F.; Tang, Y.J.; Su, B.X.; Zhou, X.H. Diverse crustal components in pyroxenite xenoliths from Junan, Sulu orogenic belt: Implications for lithospheric modification invoked by continental subduction. *Chem. Geol.* **2013**, *356*, 181–192. [CrossRef]
26. Su, B.X.; Chung, S.L.; Zarrinkoub, M.H.; Pang, K.N.; Chen, L.; Ji, W.Q.; Brewer, A.; Ying, J.F.; Khatib, M.M. Composition and structure of the lithospheric mantle beneath NE Iran: Constraints from mantle xenoliths. *Lithos* **2014**, *202–203*, 267–282. [CrossRef]
27. Downes, H. Origin and significance of spinel and garnet pyroxenites in the shallow lithospheric mantle: Ultramafic massifs in orogenic belts in Western Europe and NW Africa. *Lithos* **2007**, *99*, 1–24. [CrossRef]
28. Borghini, G.; Rampone, E.; Zanetti, A.; Class, C.; Cipriani, A.; Hofmann, A.W.; Goldstein, S.L. Pyroxenite Layers in the Northern Apennines' Upper Mantle (Italy)-Generation by Pyroxenite Melting and Melt Infiltration. *J. Petrol.* **2016**, *57*, 625–653. [CrossRef]
29. Liu, Y.S.; Gao, S.; Lee, C.T.; Hu, S.H.; Liu, X.M.; Yuan, H.L. Melt-peridotite interactions: Links between garnet pyroxenite and high Mg# signature of Continental crust. *Earth Planet. Sci. Lett.* **2005**, *234*, 39–57.
30. Marchesi, G.; Garrido, C.J.; Bosch, D.; Bodinier, J.L.; Gervilla, F.; Hidas, K. Mantle refertilization by melts of crustal-derived garnet pyroxenite: Evidence from the Ronda peridotite massif, southern Spain. *Earth Planet. Sci. Lett.* **2013**, *362*, 66–75. [CrossRef]
31. Zhang, H.F.; Deloule, E.; Tang, Y.J.; Ying, J.F. Melt/rock interaction in remains of refertilized Archean lithospheric mantle in Jiaodong Peninsula, North China Craton: Li isotopic evidence. *Contrib. Miner. Petrol.* **2010b**, *160*, 261–277. [CrossRef]
32. Seyler, M.; Lorand, J.P.; Dick, H.J.B.; Drouin, M. Pervasive melt percolation reactions in ultra-depleted refractory harzburgites at the Mid-Atlantic Ridge, 15°2′ N: ODP hole 1274A. *Contrib. Miner. Petrol.* **2007**, *153*, 303–319. [CrossRef]
33. Mercier, J.; Vergely, P.; Bebien, J. Les Ophiolites helléniques "obductées" au Jurassique supérieur sont-elles les vestiges d' un océan Tethysien ou d' une mer marginale péri-européenne ? *C.R. Somm. Soc. Geol. Fr.* **1975**, *4*, 108–112.
34. Economou, M. A short note on the evolution of the Vermion ophiolite complex (Macedonia-Greece). *Ofioliti* **1983**, *8*, 333–338.
35. Michailidis, K.M. Zoned chromites with high Mn-contents in the Fe-Ni-Cr-laterite ore deposits from the Edessa area in Northern Greece. *Miner. Deposita* **1990**, *25*, 190–197. [CrossRef]
36. Economou-Eliopoulos, M. Apatite and Mn. Zn. Co-enriched chromite in Ni-laterites of northern Greece and their genetic significance. *J. Geochem. Explor.* **2003**, *80*, 41–54. [CrossRef]
37. Tsoupas, G.; Economou-Eliopoulos, M. High PGE contents and extremely abundant PGE-minerals hosted in chromitites from the Veria ophiolite complex. Northern Greece. *Ore Geol. Rev.* **2008**, *33*, 3–19. [CrossRef]
38. Pirard, C.; Hermann, J.; O'Neill, H.S.C. Petrology and Geochemistry of the Crust-Mantle Boundary in a Nascent Arc, Massif du Sud Ophiolite, New Caledonia, SW Pacific. *J. Petrol.* **2013**, *54*, 1759–1792. [CrossRef]
39. De Hoog, J.C.M.; Gall, L.; Cornell, D. Trace element geochemistry of mantle olivine and applications to mantle petrogenesis and geothermobarometry. *Chem. Geol.* **2010**, *270*, 196–215. [CrossRef]
40. Dick, H.J.B.; Bullen, T. Chromian spinel as a petrogenetic indicator in abyssal and alpine-type peridotites and spatially associated lavas. *Contrib. Mineral. Petrol.* **1984**, *86*, 54–76. [CrossRef]
41. Arai, S. Chemistry of chromian spinel in volcanic rocks as a potential guide to magma chemistry. *Mineral. Mag.* **1992**, *56*, 173–184. [CrossRef]
42. Jan, M.Q.; Windley, B.F. Chromian spinel-silicate chemistry in ultramafic rocks of the Jijal complex, Northwestern Pakistan. *J. Petrol.* **1990**, *31*, 667–715. [CrossRef]
43. Kamenetsky, V.S.; Crawford, A.J.; Meffre, S. Factors controlling chemistry of magmatic spinel: An empirical study of associated olivine, Cr-spinel and melt inclusions from primitive rocks. *J. Petrol.* **2011**, *42*, 655–671. [CrossRef]
44. Gravestock, P.J. The Chemical Causes of Uppermost Mantle Heterogeneities. Ph.D. Thesis, Open University, Milton Keynes, UK, 1992; p. 299.
45. Santos, J.F.; Schärer, U.; Gil Ibargughi, J.I.; Girardeau, J. Genesis of Pyroxenite-rich Peridotite at Cabo Ortegal (NW Spain): Geochemical and Pb-Sr-Nd Isotope Data. *J. Petrol.* **2002**, *43*, 17–43. [CrossRef]
46. McDonough, W.F.; Sun, S.S. The composition of the Earth. *Chem. Geol.* **1995**, *120*, 223–253. [CrossRef]
47. Wood, B.; Banno, S. Garnet-orthopyroxene and orthopyroxene-clinopyroxene relationships in simple and complex systems. *Contrib. Mineral. Petrol.* **1973**, *42*, 109–124. [CrossRef]

48. Kaczmarek, M.A.; Müntener, O. Juxtaposition of melt impregnation and high temperature shear zones in the upper mantle. Field and petrological constraints from the Lanzo peridotite, (N-Italy). *J. Petrol.* **2008**, *49*, 2187–2220. [CrossRef]
49. Suhr, G.; Kelemen, P.; Paulick, H. Microstructures in Hole 1274A peridotites, ODP Leg 209, Mid-Atlantic Ridge: Tracking the fact of melts percolating in peridotite as the lithosphere is intercepted. *Geochem. Geophys.* **2008**, *9*, 1–23. [CrossRef]
50. Kelemen, P.B.; Hart, S.R.; Bernstein, S. Silica enrichment in the continental upper mantle via melt/rock reaction. *Earth Planet Sci. Lett.* **1998**, *164*, 387–406. [CrossRef]
51. Le Roux, V.; Bodinier, J.L.; Tommasi, A.; Alard, O.; Dautria, J.M.; Vauchez, A.; Riches, A.J.V. The Lherz spinel lherzolite: Refertilized rather than pristine mantle. *Earth Planet Sci. Lett.* **2007**, *259*, 599–612. [CrossRef]
52. Garrido, C.J.; Bodinier, J.L. Diversity of mafic rocks in the Ronda peridotite: Evidence for pervasive melt-rock reaction during heating of subcontinental lithosphere by upwelling asthenosphere. *J. Petrol.* **1999**, *40*, 729–754. [CrossRef]
53. Soustelle, V.; Tommasi, A.; Bodinier, J.L.; Garrido, C.J.; Vauchez, A. Deformation and reactive melt transport in the mantle lithosphere above a large-scale partial melting domain: The Ronda Peridotite Massif, Southern Spain. *J. Petrol.* **2009**, *50*, 1235–1266. [CrossRef]
54. Tilhac, R.; Ceuleneer, G.; Griffin, W.L.; O'Reilly, S.; Pearson, N.J.; Benoit, M.; Henry, H.; Girardeau, J.; Grégoire, M. Primitive Arc Magmatism and Delamination: Petrology and Geochemistry of Pyroxenites from the Cabo Ortegal Complex, Spain. *J. Petrol.* **2016**, *57*, 1921–1954. [CrossRef]
55. Laukert, G.; Handt, A.V.D.; Hellebrand, E.; Snow, J.E.; Hoppe, P.; Klügel, A. High-pressure Reactive Melt Stagnation Recorded in Abyssal Pyroxenites from the Ultraslow-spreading Lena Trough, arctic Ocean. *J. Petrol.* **2014**, *55*, 427–458. [CrossRef]
56. Schiano, P.; Clocchiatti, R.; Shimizu, N.; Maury, R.C.; Jochum, K.P.; Hofmann, A.W. Hydrous silica-rich melts in the sub-arc mantle and their relationships with erupted arc lavas. *Nature* **1995**, *377*, 595–600. [CrossRef]
57. Prouteau, G.; Scaillet, B.; Pichavant, M.; Maury, R. Evidence for mantle metasomatism by hydrous silicic melts derived from subducted oceanic crust. *Nature* **2001**, *410*, 197–200. [CrossRef] [PubMed]
58. Manning, C.E. The chemistry of subduction zone fluids. *Earth Planet Sci. Lett.* **2004**, *223*, 1–16. [CrossRef]
59. Hermann, J.; Spandler, C.; Hack, A.; Korsakov, A.V. Aqueous fluids and hydrous melts in high-pressure rocks: Implications for element transfer in subduction zone. *Lithos* **2006**, *92*, 399–417. [CrossRef]
60. Arai, S.; Takada, S.; Michibayashi, K.; Kida, M. Petrology of peridotite xenoliths from Iraya Volcano, Philippines, and implication for dynamic mantle-wedge processes. *J. Petrol.* **2004**, *45*, 369–389. [CrossRef]
61. Downes, H.; Macdonald, R.; Upton, B.G.J.; Cox, K.G.; Bodinier, J-L.; Mason, P.R.D.; James, D.; Hill, P.G.; Hearn, B.C., Jr. Ultramafic xenoliths from the Bearpaw Mountains, Montana, USA: Evidence for multiple metasomatic events in the lithospheric mantle beneath the Wyoming craton. *J. Petrol.* **2004**, *45*, 1631–1662. [CrossRef]
62. Ishimaru, S.; Arai, S. Peculiar Mg-Ca-Si metasomatism along a shear zone within the mantle wedge: Inference from fine-grained xenoliths from Avacha volcano, Kamchatka. *Contr. Mineral. Petrol.* **2011**, *161*, 703–720. [CrossRef]
63. Soustelle, V.; Tommasi, A.; Demouchy, S.; Ionov, D.A. Deformation and Fluid-Rock Interaction in the Supra-subduction Mantle: Microstructures and Water Contents in Peridotite Xenoliths from the Avacha volcano, Kamchatka. *J. Petrol.* **2010**, *51*, 363–394. [CrossRef]
64. Malaspina, N.; Herman, J.; Scambelluri, M.; Compagnoni, R. Polyphase inclusions in garnet-orthopyroxenite (Dabie Shan, China) as monitors for metasomatism and fluid-related trace element transfer in subduction zone. *Earth Planet Sci. Lett.* **2006**, *249*, 173–187. [CrossRef]
65. Vrijmoed, J.C.; Austrheim, H.; John, T.; Hin, R.C.; Corfu, F.; Davies, G.R. Metasomatism in the ultrahigh-pressure Svarberget garnet-peridotite (Western Gneiss Region, Norway): Implications for the transport of crust derived-fluids within the mantle. *J. Petrol.* **2013**, *54*, 1815–1848. [CrossRef]
66. Milke, R.; Kolzer, K.; Koch-Müller, M.; Wunder, B. Orthopyroxene rim growth between olivine and quartz at low temperatures (750–950 °C) and low water concentration. *Minerl. Petrol.* **2009**, *97*, 223–232. [CrossRef]
67. Milke, R.; Abart, R.; Keller, L.; Rhede, D. The behavior of Mg, Fe and Ni during the replacement of olivine dy orthopyroxene: Experiments relevant to mantle metasomatism. *Minerl. Petrol.* **2011**, *103*, 1–8. [CrossRef]

68. Gardés, E.; Wunder, B.; Marquardt, K.; Heinrich, W. The effect of water on intergranular mass transport: New insights from diffusion-controlled reaction rims in the MgO-SiO_2 system. *Contr. Mineral. Petrol.* **2012**, *164*, 1–16. [CrossRef]
69. Grant, T.B.; Harlov, D.E.; Rhede, D. Special collection: New advances in subduction zone magma genesis: Experimental formation of pyroxenite veins by reactions between olivine and Si, Al, Ca, Na, and Cl-rich fluids at 800 °C and 800 MPa: Implications for fluid metasomatism in the mantle wedge. *Am. Mineral.* **2016**, *101*, 808–818. [CrossRef]
70. Smith, D.; Riter, J.C.A.; Mertzman, S.A. Water-rock interactions, orthopyroxene growth, and Si-enrichment in the mantle: Evidence in xenoliths from Colorado Plateau, southwestern United States. *Earth Planet Sci. Lett.* **1999**, *165*, 45–54. [CrossRef]
71. McInnes, B.I.A.; Gregoire, M.; Binns, R.A.; Herzig, P.M.; Hannington, M.D. Hydrous metasomatism of oceanic sub-arc mantle, Lihir, Papua New Guinea: Petrology and geochemistry of fluid-metasomatised mantle wedge xenoliths. *Earth Planet Sci. Lett.* **2001**, *188*, 169–183. [CrossRef]
72. Arai, S.; Miura, M. Formation and modification of chromitites in the mantle. *Lithos* **2016**, *264*, 277–295. [CrossRef]
73. Barth, M.G.; Mason, P.; Davies, G.R.; Drury, M.R. The Othris Ophiolite, Greece: A snapshot of subduction initiation at a mid-ocean ridge. *Lithos* **2008**, *100*, 234–254. [CrossRef]
74. Bizimis, M.; Salters, V.; Bonatti, E. Trace and REE content of clinopyroxenes from supra-subduction zone peridotites. Implications for melting and enrichment processes in island arcs. *Chem. Geol.* **2000**, *165*, 67–85. [CrossRef]
75. Ulrich, M.; Picard, C.; Guillot, S.; Chauvel, C.; Cluzel, D.; Meffre, S. Multiple melting stages and refertilization as indicators for ridge to subduction formation: The New Caledonia ophiolite. *Lithos* **2010**, *115*, 223–236. [CrossRef]
76. König, S.; Münker, C.; Schuth, S.; Luguet, A.; Hoffmann, J.E.; Kuduon, J. Boninites as windows into trace element mobility in subduction zones. *Geochim. Cosmochic. Acta* **2010**, *74*, 684–704. [CrossRef]
77. Cluzel, D.; Ulrich, M.; Jourdan, F.; Meffre, S.; Paquette, J.L.; Audet, M.A.; Secchiari, A.; Maurizot, P. Early Eocene clinoenstatite boninite and boninite-series dikes of the ophiolite of New Caledonia; a witness of slab-derived enrichment of the mantle wedge in a nascent volcanic arc. *Lithos* **2016**, *260*, 429–442. [CrossRef]
78. Deschamps, F.; Godard, M.; Guillot, S.; Hattori, K. Geochemistry of subduction zone serpentinites: A review. *Lithos* **2013**, *178*, 96–127. [CrossRef]
79. Müntener, O.; Kelemen, P.B.; Grove, T.L. The role of H_2O during crystallization of primitive arc magmas under uppermost mantle conditions and genesis of igneous pyroxenites: An experimental study. *Contr. Mineral. Petrol.* **2001**, *141*, 643–658. [CrossRef]
80. Zangana, N.A.; Downes, H.; Thirlwall, M.F.; Hegner, E. Relationship between deformation, equilibration temperatures, REE and radiogenic isotopes in mantle xenoliths (Ray Pic, Massif Central, France): An example of plume-lithosphere interaction? *Contr. Mineral. Petrol.* **1997**, *39*, 1917–1930. [CrossRef]
81. Barsdell, M.; Berry, R.F. Origin and evolution of primitive island arc ankaramites from Western Epi, Vanuatu. *J. Petrol.* **1990**, *31*, 747–777. [CrossRef]
82. Eggins, S.M. Origin and differentiation of picritic arc lavas from Aoba (Ambae), Vanuatu. *Contrib. Mineral. Petrol.* **1993**, *114*, 79–100. [CrossRef]
83. Ionov, D.A.; Dupuy, C.; O'Reilly, S.Y.; Kopylova, M.G.; Genshaft, Y.S. Carbonated peridotite xenoliths from Spitsbergen: Implications for trace elements signature of mantle carbonate metasomatism. *Earth Planet Sci. Lett.* **1993**, *119*, 283–297. [CrossRef]
84. Yaxley, G.M.; Green, D.H.; Kamenetsky, V. Carbonatite metasomatism in southern Australia lithosphere. *J. Petrol.* **1998**, *39*, 1917–1930. [CrossRef]
85. Downes, H. Formation and modification of the shallow subcontinental lithospheric mantle: A review of geochemical evidence from ultramafic xenolith suites and tectonically emplaced ultramafic massifs of Western and Central Europe. *J. Petrol.* **2001**, *42*, 233–250. [CrossRef]
86. Tsikouras, B.; Karipi, S.; Rigopoulos, I.; Perraki, M.; Pomonis, P.; Hatzipanagiotou, K. Geochemical processes and petrogenetic evolution of rodingite dykes in the ophiolite complex of Othrys (Central Greece). *Lithos* **2009**, *113*, 540–554. [CrossRef]
87. Tsikouras, B.; Karipi, S.; Hatzipanagiotou, K. Evolution of rodingites along stratigraphic depth in the Iti and Kallidromon ophiolites (Central Greece). *Lithos* **2013**, *175–176*, 16–29. [CrossRef]

88. Green, D.H.; Fallon, T.J. Pyrolite: A Ringwood concept and its current expression. In *The Earth's Mantle: Composition, Structure and Evolution*; Jackson, I.N.S., Ed.; Cambridge University Press: Cambridge, UK, 1998; pp. 331–380.
89. Schmidt, M.W.; Green, D.H.; Hibberson, W.O. Ultracalcic magmas generated from Ca-depleted mantle: An experimental study on the origin of ankaramites. *J. Petrol.* **2004**, *45*, 531–554. [CrossRef]
90. Green, D.H.; Schmidt, M.W.; Hibberson, W.O. Island-arc ankaramites: Primitive melts from fluxed refractory lherzolitic mantle. *J. Petrol.* **2004**, *45*, 391–403. [CrossRef]
91. Koloskov, A.V.; Zharinov, S.E. Multivariate statistical analysis of clinopyroxene compositions from mafic and ultramafic xenoliths in volcanic rocks. *J. Petrol.* **1993**, *34*, 173–185. [CrossRef]
92. Buccianti, A.; Vaselli, O. An introduction to the multivariate statistical analysis of compositional data: Applications to classification problems of clinopyroxenes from mafic and ultramafic rocks. *Mineral. Petrogr. Acta* **1996**, *39*, 275–289.
93. Parkinson, I.J.; Pearce, J.A. Peridotites from the Izu-Bonin-Mariana forearc (ODP Leg 125): Evidence for mantle melting and melt-mantle interaction in a supra-subduction zone setting. *J. Petrol.* **1998**, *39*, 1577–1618. [CrossRef]
94. Obata, M. Petrology and Petrogenesis of the Ronda High-Temperature Peridotite Intrusion, Southern Spain. Ph.D. Thesis, Massachusetts Institute of Technology, Cambridge, MA, USA, 1977; p. 247.
95. Gaggero, L.; Cortesogno, L. Metamorphic evolution of oceanic gabbros: Recrystallization from solidus to hydrothermal conditions in the MARK area (ODP Leg 153). *Litthos* **1997**, *40*, 105–131. [CrossRef]
96. Flower, M.F.J.; Robinson, P.T.; Schmincke, H.U.; Ohnmacht, W. Magma fractionation systems beneath the Mid-Atlantic ridge at 36–37-N. *Contrib. Mineral. Petrol.* **1977**, *74*, 361–374. [CrossRef]
97. Singh, A.K.; Nayak, R.; Khogenkumar, S.; Subramanyam, K.S.V.; Thakur, S.S.; Singh, R.K.B.; Satyanarayanan, M. Genesis and tectonic implications of cumulate pyroxenites and tectonite peridotites from the Nagaland-Manipur ophiolites, Northeast India: Constraints from mineralogical and geochemical characteristics. *Geol. J.* **2016**. [CrossRef]
98. Uysal, I.; Ersoy, Y.E.; Dilek, Y.; Kapsiotis, A.; Sarifakioglu, E. Multiple episodes of partial melting, depletion, metasomatism and enrichment processes recorded in the heterogeneous upper mantle sequence of the Neotethyan Eldivan ophiolite, Turkey. *Lithos* **2016**, *246–247*, 228–245. [CrossRef]